International Journal of Chemical Studies

P-ISSN: 2349–8528
E-ISSN: 2321–4902
www.chemijournal.com
IJCS 2023; 11(1): 133-139

Received: 23-11-2022
Accepted: 28-12-2022

Rajeev Ranjan Deo Pandey
University Department of Physics, Ranchi University, Ranchi, Jharkhand, India

Sumit Kaur
Department of Physics, Nirmala College, Ranchi University Ranchi, Jharkhand, India

Binay Prakash Akhouri
Department of Physics, Suraj Singh Memorial, College, Ranchi, Jharkhand, India

Corresponding Author:
Binay Prakash Akhouri
Department of Physics, Suraj Singh Memorial, College, Ranchi, Jharkhand, India

Study of axis symmetric shapes of sessile drops

Rajeev Ranjan Deo Pandey, Sumit Kaur and Binay Prakash Akhouri

Abstract
By fitting the Laplacian equation of capillarity to the dimensions of sessile drops, axis symmetric drop shape analysis (ADSA) techniques are presented for the computations of any one (the contact angle, the interfacial tension, and the radius of curvature at the drop apex) if the values of two other are known. With the change of area of pendant drops, the change in Gibb's energy and the change in work done are computed. Numerically generated drop profiles used to demonstrate the accuracy and applicability of the method.

Keywords: Surface tension, axis symmetric drop shape analysis (ADSA), sessile drops

Introduction

Surface tension is the boundary tension at a liquid-gas interface. The boundary tension at a liquid–liquid contact is termed as interfacial tension. The determination of liquid-gas surface tension and liquid-liquid interfacial tension is essential in a number of scientific and industrial fields. The capillary rise method [1-4], the do Noisy ring method [5-7], the Wilhelmy plate method [8, 9], the height of a meniscus on a vertical plane method [10, 27], the spinning drop method [11, 12], the maximum bubble pressure method [13, 14], the drop weight method [15,16], and the drop or bubble shape analysis method [1-16] have all been developed to measure surface/interfacial tension. Among these methods, drop shape analysis method has a number of advantages. The measurement of interfacial tension using drop form methods is powerful, diverse, and adaptable. While studying liquid-fluid menisci, Neumann and colleagues established the axis symmetric drop shape analysis (ADSA) numerical technique [17-18] for calculating surface and interfacial tensions from the shape of drops or bubbles.

Today, ADSA [17-18] has been widely used in a variety of applications, including cellular biomechanics and oil recovery. Bash forth and Adams [20] developed sessile drop profiles for different surface tensions and radii of curvature at the apex of the drop, which was the first study in the field of axis symmetric drops analysis. Maze and Burnet [21] devised a more precise approach for determining interfacial tensions based on the shape of sessile drops.

Further development of DSA techniques [17-36] are ADSA-P [17-18], ADSA-NA (No apex) [17], ADSA-CSD (constrained sessile drop) [17], ADSA-D(diameter) [17], ADSA-HD (height and diameter) [22], ADSA –TD(two diameter) [30], ADSA-CB (captive bubble) [17-20], and ADSA-EF (electric field) [17]. The ADSA-EFis applicable to pendant and sessile drops/bubbles. For studying accuracy of drop shape techniques the geometrical shape parameters and physical dependence of shape parameters are primarily investigated.

In order to analyse physical dependence of shape parameters, the limitations of four drop shapes categories are principally presented which are, volume-radius limited [18], Volume-angled limited [18], volume-radius-radius limited [18] and the volume-radius-angle limited [18]. For measuring interfacial tension, however, the approaches indicated above are more powerful, diverse, and adaptable.

For determining interfacial tension, a variety of approaches have been presented. There is currently a large body of literature documenting the new approaches as well as enhancements to old methods. However, only a few are of outstanding importance. We will discuss among them the most fundamental method i.e., the method for computing the interfacial tension from the shapes of sessile drops.

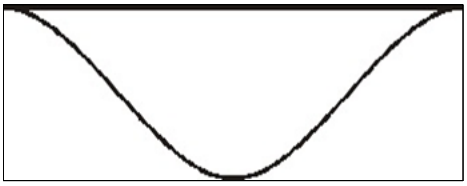

(i) A pendant drop

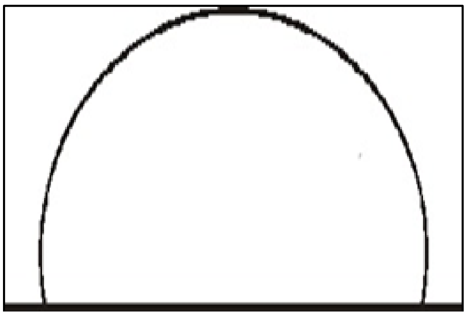

(ii) A sessile drop

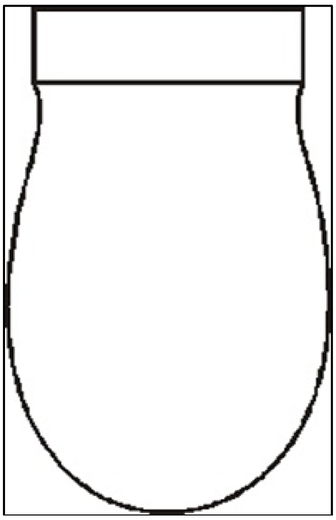

(iii) A pendant drop with a cylindrical tip

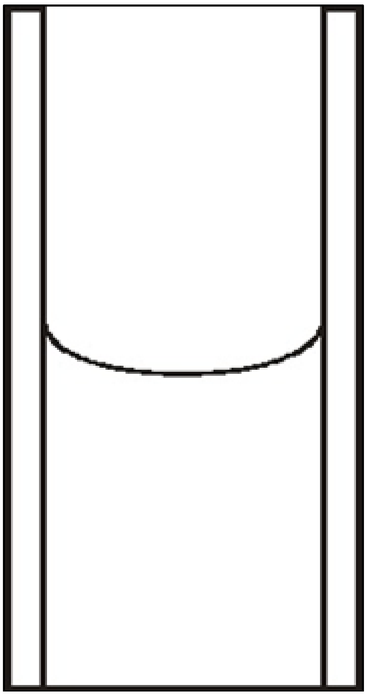

(iv) A sessile drop in a capillary tube

Fig 1: Gives apresentation of a pendant and a sessile drop.

Pendant drops results (i) when the liquid drop is hanging from a flat, horizontal surface, or (ii) from a vertical cylindrical tip. Sessile drops are shaped like an oblate spheroid. They are formed (iii) when a drop of liquid settles on a flat, horizontal plate, or (iv) The liquid surface in a capillary tube also has the sessile shape. Pendant drops correspond to a prolate spheroid. The balance between surface tension and extrinsic forces, such as gravity, determines the shape of the drop/bubble. Gravity deforms the drop, elongating a pendant drop or flattening a sessile drop, whilst surface tension tries to round it. When the surface tension effect is substantially greater than the gravitational influence, the shape of both pendent and sessile drops/bubbles tends to become spherical. Theoretically, each drop shape corresponds to a constant surface tension value. A little change in surface tension generates a large change in shape for well-defined geometries. A considerable change in surface tension, on the other hand, generates just a modest change in shape for approximately spherical drop/bubble geometries. The connection between drop shape and surface tension lies at the heart of drop shape methods. The Laplace equation of capillarity includes this information. The drop shapes as in Figure 2 can be generated using a Laplace equation.

Theory

When a drop of liquid with interfacial tension γ is placed on a non-wetting solid surface, the drop assumes a shape that is determined by the contact angle θ_c that the liquid makes at the three-phase contact line, in accordance with the Young–Dupré equation (see) [19]. Under static conditions, the drop shape must also satisfy the Young–Laplace equation of capillarity [37-38], which describes the mechanical equilibrium conditions for two homogeneous fluids separated by an interface:

$$\gamma\left(\frac{1}{R_1}+\frac{1}{R_2}\right)=\Delta P \qquad (1)$$

Where R_1 and R_2 are the two principal radii of curvature, γ is the liquid –fluid interfacial tension, and ΔP is the pressure difference across the interface. In the absence of external forces other than gravity, the pressure difference is a linear function of the elevation:

$$\Delta P=\Delta P_0+(\Delta\rho)\,gz \qquad (2)$$

Where ΔP_0 is the pressure difference at a reference plane, $\Delta\rho$ is the density difference between the two bulk phase, g is the gravitational acceleration, and z is the vertical height of the given point on the drop surface, measured from the reference level. The integration of the Laplace equation (1) is straightforward only for a cylindrical meniscii, i.e., menisci for which one of the principal radii of curvatures is zero. For a general irregular meniscus, numerical integration would be very difficult. For the specific case of axis-symmetric drops, e.g. sessile drops and pendant drop drops, numerical procedures have been devised [17-18]. Fortunately obtaining axial symmetry is not difficult for most sessile drop and pendant drop systems. For the axial symmetry of the interface, the curvature at the apex is constant in all directions and the two radii of curvature are equal, i.e,

$$\frac{1}{R_0} = \frac{1}{R_1} = \frac{1}{R_2} = b \qquad (3)$$

At $s = 0$, where R_0 and b are the radius of curvature and the curvature at the origin($x = 0$ and $z = 0$ as shown in Fig.2) respectively. Then, from equation (1), the pressure difference at the origin can be expressed as

$$\Delta P_0 = 2b\gamma \qquad (4)$$

Using equation (1), (2) and(3) we have the following form of Laplace equation:

$$\gamma\left(\frac{1}{R_1} + \frac{1}{R_2}\right) = 2b\gamma + (\Delta\rho)\, gz \qquad (5)$$

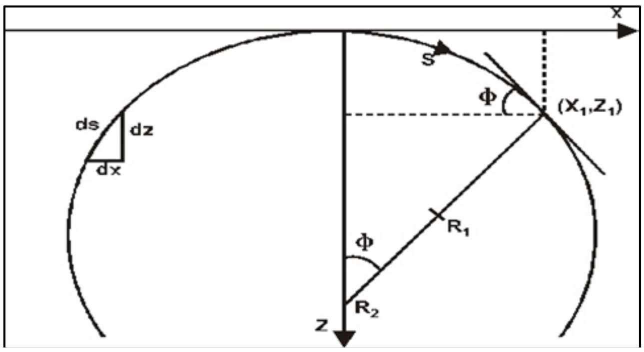

Fig 2: Axis symmetric co-ordinate system

In this work, the shape of an axis-symmetric sessile drop is computed for given γ, $b = 1/R_0$, and contact angle θ_c. The liquid is taken to be water and the surrounding fluid is air. For computational purposes it is convenient to work with arc length *s* along the curve and the turning angle ϕ, which is defined in terms of the local slope by $dz/dx = \tan\phi$. Introducing ϕ and the arc length *s* (i.e., $ds = \sqrt{dx^2 + dy^2}$) as new variables along the interface allows the Young–Laplace equation to be expressed as $d\phi/ds = 2b + cz - \sin\phi/x$ with $dx/ds = \cos\phi$, $dy/ds = \sin\phi$, and $dA/ds = 2\pi x$ and $dV/ds = \pi x^2 \sin\phi$; where *V* is the volume and *A* the surface area of the drop. Thus for a given γ and θ_c, specifying the reference curvature b is equivalent to specifying the volume or surface area of the drop. *V* (or *A*) decreases monotonically with increasing b. The capillary constant *c* has positive values for sessile drops and negative values for pendant drop and is expressed as $c = (\Delta\rho)g/\gamma$. Here, $\Delta\rho = 997.38$ Kg/m^3 and $g = 9.8 m/s^2$.

Result and discussion

In numerically generated Figures 3(*a*)-3(*g*), we find that the curved surfaces changes, i.e., either moves outwards or inwards depending mainly on the values of the three parameters viz the contact angle θ_c, the interfacial tension γ, and the radius of curvature R_0 at the drop apex. The parameterizations of the different quantities are as follows: $0 < s < 4$, $0 < \theta_c < 180^0$, $0 < \gamma < 72$, $-0.8 < 1/R_0 < 0$ and $0.6 < x < 6$ and $0 < y < -0.37$. For numerical evaluation of the drops the initial conditions used were set as: $\phi(0) = 0, z(0) = 0, x(0) = 0, V(0) = 0$ and $A(0) = 0.$

$$\gamma = 50, \theta_c = 30^0, 1/R_0 = -5.05$$

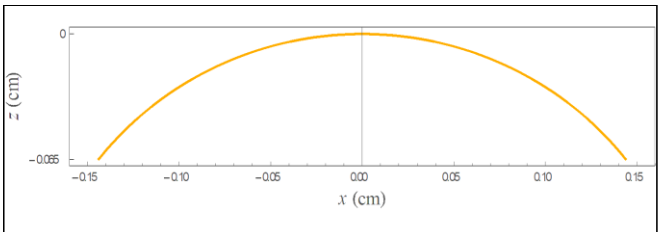

Fig (a)

$$\gamma = 50, \theta_c = 50^0, 1/R_0 = -5.05$$

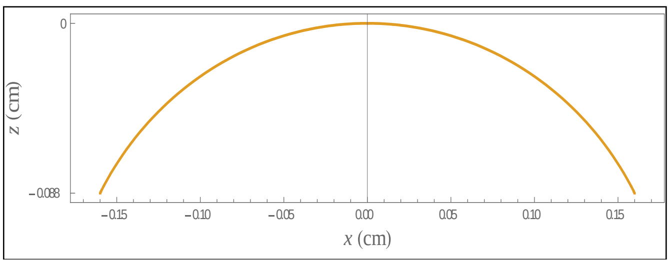

Fig (b)

$$\gamma = 50, \theta_c = 60^0, 1/R_0 = -5.05$$

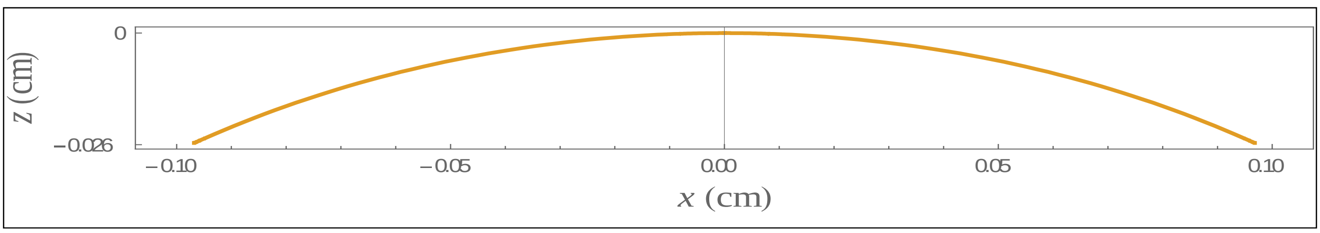

Fig (c)

$$\gamma = 50, \theta_c = 90^0, 1/R_0 = -5.05$$

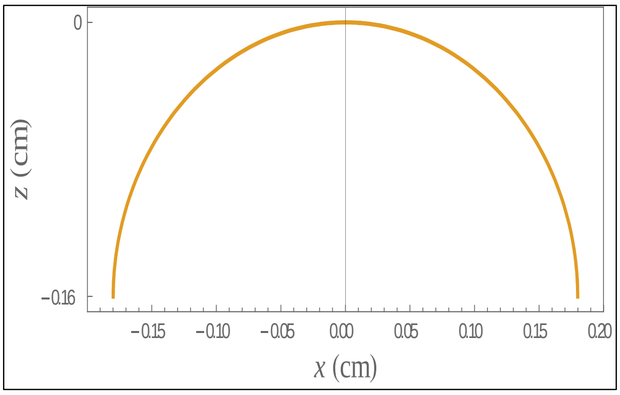

Fig (d)

$$\gamma = 50, \theta_c = 120^0, 1/R_0 = -5.05$$

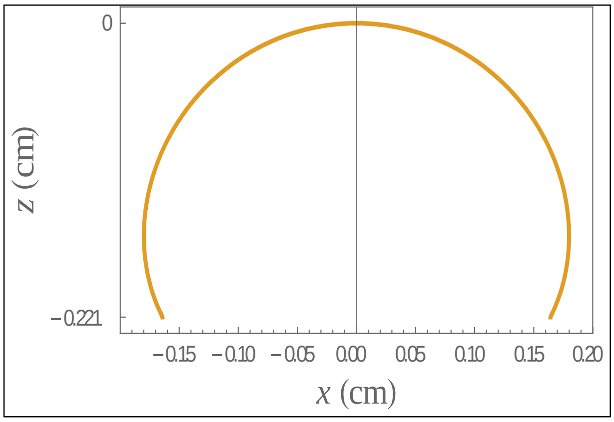

Fig (e)

$$\gamma = 50, \theta_c = 150^0, 1/R_0 = -5.05$$

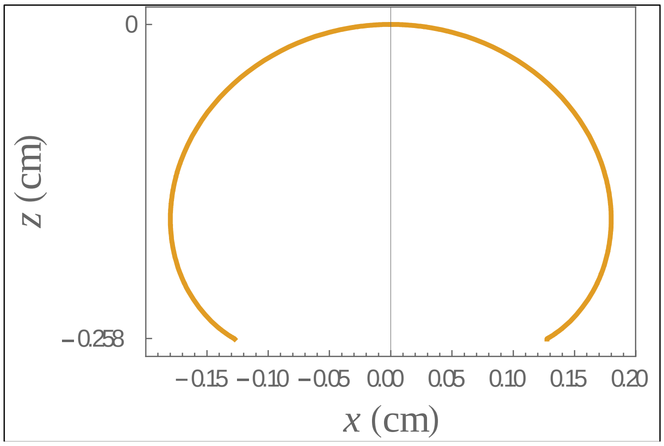

Fig (f)

$$\gamma = 50, \theta_c = 180^0, 1/R_0 = -5.05$$

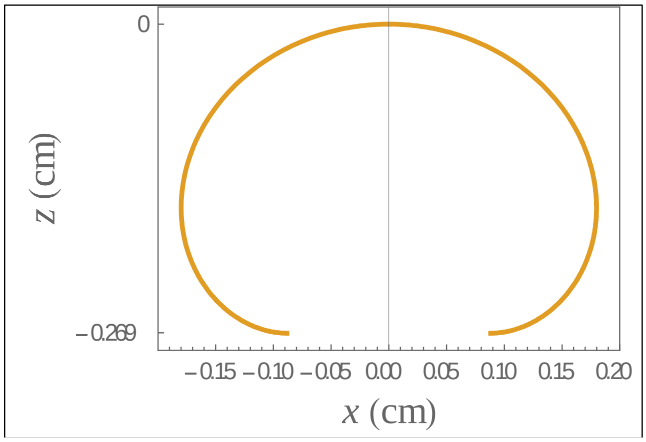

Fig (g)

Fig 3 (a) to 3(g): Shapes of an axis-symmetric sessile drop with varying contact angles (see Table1)

Table 1: Volume, area, height and contact radius of a sessile drop with varying θ_c

$1/R_0$ (m^{-1})	γ N/m	θ_c in degree	Volume $10^{-8} \times m^3$	Area $10^{-6} \times m^2$	Height $10^{-4} \times m$	Contact radius $10^{-4} \times m$
-5.05	50	30	0.0387	3.1490	2.5605	9.6760
		50	0.2270	7.8344	6.4761	14.3705
		60	0.3960	10.5424	8.7917	15.9948
		90	0.0775	18.7733	16.0047	17.9871
		120	1.6625	25.7547	22.0932	16.4049
		150	1.92402	30.6558	25.8273	12.7370
		180	1.96976	33.4525	26.9333	8.82637

Table 2: Volume, area, height and contact radius of a sessile drop with varying θ_c

$1/R_0$ m^{-1}	γ N/m	θ_c in degree	Volume $10^{-8} \times m^3$	Area $10^{-6} \times m^2$	Height $10^{-4} \times m$	Contact radius $10^{-4} \times m$
-1.05	30	30	1.24664	34.2627	7.0566	32.1440
		50	3.8739	56.9196	13.3310	39.8270
		60	5.4525	66.3540	16.3274	40.9361
		90	10.1674	89.1619	24.2758	44.2037
		120	13.7148	106.097	30.1816	42.6894
		150	15.5983	119.0020	33.7011	39.7011
		180	16.1032	129.013	34.8199	35.1444
	50	30	1.7377	41.9625	8.1797	35.5154
		50	5.9050	73.8862	16.0693	45.604

		60	85.1153	87.5740	19.8907	47.8497
		90	16.4582	121.1130	30.0092	50.7571
		120	22.4606	146.1000	37.691	48.8089
		150	25.5937	164.937	42.2066	44.3653
		180	26.4094	179.238	43.6318	39.1787
	70	30	2.0209	47.0563	8.89739	37.5716
		50	7.6027	86.3779	17.9916	48.6733
		60	11.1558	103.6440	22.4532	51.8126
		90	22.1749	146.4450	34.4382	55.2248
		120	30.5317	178.4490	43.3935	52.9287
		150	34.8386	202.391	48.7065	47.7024
		180	35.9347	220.2650	50.3743	41.6424

Table 3: Volume, area, height and contact radius of a sessile drop with varying θ_c

$1/R_0$ m^{-1}	γ N/m	θ_c **in degree**	**Volume** $10^{-8}\times m^3$	**Area** $10^{-6}\times m^2$	**Height** $10^{-4}\times m$	**Contact radius** $10^{-4}\times m$
-4.15	30	30	0.06300	4.3845	2.9750	11.4255
		50	0.3302	10.1659	7.1347	16.4391
		60	0.5478	13.2374	9.4459	18.0624
		90	1.34164	21.8473	16.2033	19.9554
		120	1.98351	28.7095	21.5654	18.5730
		150	2.2846	33.5993	24.7684	15.4281
		180	2.34681	36.7349	25.7347	11.9698
	50	30	0.06735	4.56585	3.0669	11.6540
		50	0.37900	11.0662	7.6045	17.1056
		60	0.64807	14.7000	10.2221	18.9426
		90	1.6888	25.3683	18.1529	21.1471
		120	2.5566	34.1598	24.6570	19.4636
		150	2.9527	40.3617	28.5901	15.6017
		180	3.0276	44.0979	29.7633	11.4298
	70	30	0.0694	4.6509	3.1098	11.7597
		50	0.4052	11.5330	7.8454	17.4388
		60	15.4924	15.4924	10.6368	19.3970
		90	1.9067	27.4706	19.2979	21.7914
		120	2.9342	37.5878	26.5780	19.9008
		150	3.3947	44.6939	31.0327	15.5253
		180	3.47622	48.7816	32.3533	10.8519

Table 4: Volume, area, height and contact radius of a sessile drop with varying θ_c

$1/R_0$ m^{-1}	γ N/m	θ_c **in degree**	**Volume** $10^{-8}\times m^3$	**Area** $10^{-6}\times m^2$	**Height** $10^{-4}\times m$	**Contact radius** $10^{-4}\times m$
-9.55	30	30	0.00595	0.9024	1.3792	5.1783
		50	0.03691	2.3227	3.5797	7.8090
		60	0.06622	3.1830	4.9286	8.7544
		90	0.19294	5.9535	9.3325	9.9570
		120	0.3076	8.4394	13.2684	8.92508
		150	0.3572	10.1833	15.7755	6.4575
		180	0.3646	11.0704	16.5149	3.8755
	50	30	00.0060	0.9104	1.38852	5.2008
		50	0.0382	2.3750	3.6407	7.8902
		60	0.0694	3.2799	5.0428	8.8726
		90	0.2090	6.2774	9.7285	10.1444
		120	0.3391	9.0550	14.0570	9.0029
		150	0.3947	11.0136	16.8967	6.2015
		180	0.4020	11.9366	17.7407	3.2793
	70	30	0.00608	9.1395	1.39256	5.2106
		50	0.0388	2.39861	3.6681	7.9364
		60	0.0709	3.32446	5.0950	8.9261
		90	0.2169	6.4342	9.9195	10.2315
		120	0.3553	9.3666	14.4572	9.0308
		150	0.4139	11.4444	17.4914	6.0320
		180	0.4211	12.3790	18.4026	2.8930

Any plane's interaction with the curved surface generates a two-dimensional curvature containing one of the two independent radii of the curved surface (R_1 and R_2). If the curved surface becomes a little larger and moves by an amount of dz, the new position of the surface will be formed. Therefore, there will be changes in surface dimensions x (abscissa), y (ordinate) and z (normal coordinate to paper plain) to $x+dx$, $y+dy$ and $z+dz$ amounts. Consequently, the changes in area, Gibbs free energy, and work will be:

$$\Delta A = (x+dx)(y+dy) - xy = xdy + ydx + dxdy \approx xdy + ydx \tag{6}$$

$$dG = \gamma(xdy + ydx) \tag{7}$$

$$W = \Delta PdV = \Delta Pxydz = \gamma(xdy + ydx) \tag{8}$$

In table 1, it can easily be observed that the contact radius increases when the contact angle values increase from 30^0 to 90^0 and decreases when the contact angle value decreases from 90^0 to 180^0 for $1/R_0 = -5.05\ (m^{-1})$, $\gamma = 50\ (N/m)$. In table2-4, it can also be observed that the same is true for every set of $1/R_0\ (m^{-1})$, $\gamma(N/m)$ and θ_c (in degree). We can also calculate the change in Gibb's energy by using equation (6) and (7). In table 1, the change in area at two contact angles 30^0 and $90^0$is $(18.7733 - 3.1490)\times 10^{-6} \approx 15.624\times 10^{-6} m^2$. Similarly, the change in area at two contact angles 90^0 and 180^0 is $(33.4525 - 18.7733)\times 10^{-6} \approx 14.699\times 10^{-6} m^2$. Hence, the change in Gibbs energy for the two cases of contact angles is $-78.90\times 10^{-6}\,Nm$ and $-74.23\times 10^{-6}\,Nm$. Bash forth and Adams [20] derived the theoretical form of sessile or pendant drop and calculated tables of drop contours. The interfacial tension of a sessile or a pendant drop was determined by matching the experimentally measured drop profile to a theoretical drop contour. However, the visual comparison of drop profiles was time-consuming, tedious and subjective.

Conclusion

The surface energy of the solid sample may be calculated using two parameters: surface energy and especially the contact angle of the liquid droplet. It has also been discovered that the sessile drop analysis approach is useful for measuring contact angles. The change in Gibb's energy is determined using volume and area calculations. The significance of these computations can be seen from the concept of interfacial tension. By definition the interfacial tension is the increase in Gibb's free energy per increase of the surface area at constant T, P and N_i.

References

1. EA Boucher. Reports on Progress in Physics. 1980;43(4):497-546 ().
2. T Liu, Jin CJ. Chang, Scientific Report. 2017;7(1):740-752().
3. VV Kashin, KM Shakirov, AI Posheneva. 2011;41(10):795-798 ().
4. F Bashforth, JC Adams. Cambridge University Press. London, England; c1883.
5. PL Du Nouy, J Gen. Physiol; c1919. p. 521-524.
6. H Zuidema, G Waters, Indus & Engineering Chemistry. 1941;13(5):312-313.
7. WD Harkins, HF Jordan. Science. 1930;72:73-75.
8. K (ed.) Holmberg, Hand book of Applied Surface and Colloid Chemistry, New York, Wiley and Sons. 2002;2:219.
9. HJ Butt, K Graf, M Kappl. Physics and Chemistry of Interfaces, Weinhelm, Wiley-VCH-Vert; c2006. p. 16.
10. D Vella, L Mahadevan, American Journal of Physics. 2005;73:817-825.
11. B Vonnegut, Rev. Sci. Insrum. 1942;13(6):6-9.
12. HH Hu, D Joshep, J. Colloid Interface Sci. 1994;162(2):331-339.
13. AW Adamson. Physical Chemistry of Surfaces VI Edition, John Wiley and Sons, New York; c1982.
14. AT Hubbard. CRC Press; c2002. p. 814-815.
15. OE Yildirim, Q Xu, OA Basaran. 2005;17:062107.
16. AW Adamson, A Gast. Physical Chemistry of Surfaces, VIth edition, Wiley New York; c1997.
17. OID Rio, AW Neumann. Journal of Colloid and Interface Science. 1997;196(2):136-147.
18. SMI Saad, A.W. Neumann, Advances in Colloid and Interface Science. 2016;238:62-87.
19. PG De Gennes, F Brochard-Wyart, D Quere. Capillarity and Wetting Phenomena, New York: Springer; c2004.
20. F Bashforth, JC Adams. Cambride University Press, London; c1883.
21. C Maze, G Barnet. Surface Science. 1969;13(2):451-470.
22. S Hartland, RW Hartley. Colloids and Surfaces. 1990;43(2):151-167.
23. AJ Amirfazil, S Graham-Eagle, S Pennell, AW Neumann. Colloids and Surfaces A: Physicochemical and Engineering Aspects. 2000;161(1):63-74.
24. WG Anderson. Journal of Petroleum Technology. 1986a;38(11):1125-1144.
25. WG Anderson. Journal of Petroleum Technology. 1986b;38(12):1246-1262.
26. PL Du Nouy. Journal of General Physiology. 1919;1(5):521-524.
27. PR Edwards. Journal of the Chemical Society. 1925;127:744-747.
28. HY Erbil. Surface Chemistry of Solid and Liquid Interfaces, Wiley-Blackwell; c2006.
29. M Hoorfar, AW Neuman. Advances in Colloid and Interface Science. 2006;121(1-3):25-49.
30. DY Kwok, CJ Budziak, AW Neumann. Journal of Colloid and Interface Science. 1995;173(1):143-150.

31. D Li, P Cheng, AW Neumann. Advances in Colloid and Interface Science. 1992;39:347-382.
32. L Wilhelmy, Annalen der Physik und Chemie. 1963;195(6):177-217.
33. A Kalantarian, H Ninomiya, SM Saad, R David, R Winklbauer, AW Neumann. Biophysical Journal. 2009;96(4):1606-161.
34. M Hoorfar, MA Kurz, AW Neumann. Colloids and Surfaces Physicochemical and Engineering Aspects. 2005;260(1-3):277-285.
35. SMI Saad, Z Policova, EJ Acosta, AW Neumann. Langmuir. 2010;26(17):14004-14013.
36. A Kalantarian, R David, J Chen, AW Neumann. Langmuir. 2011;27(7):3485-3495.
37. T Young. Philosophical Transactions of the Royal Society of London. 1805;95:65-67.
38. PS Marquis de Laplace, Traité de Mécanique Céleste, (Paris, France: Courcier); c1805. Volume 4.